International Journal of Numerical Methods for Heat & Fluid Flow

Heat and mass transfer analysis in natural convection flow of nanofluid over a vertical cone with chemical reaction

P. Sudarsana Reddy A. Chamkha

The current issue and full text archive of this journal is available on Emerald Insight at:
www.emeraldinsight.com/0961-5539.htm

Received 6 October 2015
Revised 15 December 2015
Accepted 17 December 2015

Heat and mass transfer analysis in natural convection flow of nanofluid over a vertical cone with chemical reaction

P. Sudarsana Reddy
Department of Mathematics, RGM College of Eng. & Tech, Nandyal, India, and
A. Chamkha
Department of Mechanical Engineering, Prince Mohammad Bin Fahd University, Al-Khobar, Saudi Arabia

Abstract

Purpose – In recent years, nanofluids are being widely used in many thermal systems because of their higher thermal conductivity and heat transfer rate. The higher thermal conductivity depends on many parameters such as size, shape and volume and the Brownian motion and thermophoresis of added nanoparticles. The purpose of this paper is to analyze the influence of the Brownian motion and thermophoresis on natural convection heat and mass transfer boundary layer flow of nanofluids over a vertical cone with radiation.

Design/methodology/approach – Using similarity variables, the non-linear partial differential equations, which represent momentum, energy and diffusion, are transformed into ordinary differential equations. The transformed conservation equations are solved numerically subject to the boundary conditions by using versatile, extensively validated, variational finite-element method.

Findings – The sway of significant parameters such as magnetic field (M), buoyancy ratio parameter (Nr), Brownian motion parameter (Nb), thermophoresis parameter (Nt), thermal radiation (R), Lewis number (Le) and chemical reaction parameter (Cr) on velocity, temperature and concentration evaluation in the boundary layer region is examined in detail. The results are compared with previously published work and are found to be in agreement. The velocity distributions are reduced, while temperature and concentration profiles elevate with a higher (M). With the improving values of (R), the velocity and temperature sketches improve, while concentration distributions are lowered in the boundary layer region. The temperature and concentration profiles are elevated in the boundary layer region for higher values of (Nt). With the increasing values of (Nb), temperature profiles are enhanced, whereas concentration profiles get depreciated in the flow region.

Social implications – In recent years, it has been found that magneto-nanofluids are significant in many areas of science and technology. It has applications in optical modulators, magnetooptical wavelength filters, tunable optical fiber filters and optical switches. Magnetic nanoparticles are especially useful in biomedicine, sink float separation, cancer therapy, etc. Specific biomedical applications involving nanofluids include hyperthermia, magnetic cell separation, drug delivery and contrast enhancement in magnetic resonance imaging.

Originality/value – To the best of the authors' knowledge, no studies have assessed the impact of the two slip effects, namely, Brownian motion and thermophoresis, on the natural convection of electrically conducted heat and mass transfer to the nanofluid boundary layer flow over a vertical cone in the presence of radiation and chemical reaction; therefore, this problem has been addressed in this study.

International Journal of Numerical Methods for Heat & Fluid Flow
Vol. 27 No. 1, 2017
pp. 2-22

0961-5539
DOI 10.1108/HFF-10-2015-0412

The authors are thankful to the reviewers for their decent suggestions and observations to improve the quality of the manuscript.

Comparison of the results of this study's with those of previously published work was found to be in good agreement.

Keywords Nanofluid, Thermophoresis, Brownian motion, Radiation, Chemical reaction, Vertical cone

Paper type Research paper

Nomenclature

g	= Gravitational acceleration vector (m/s^2)
K_m	= Thermal conductivity (W m^{-1} K^{-1})
C	= Nanoparticle volume fraction
C_∞	= Ambient nanoparticle volume fraction
T_w	= Temperature at the cone surface
T	= Fluid temperature (K)
q_w	= Wall heat flux
D_B	= Brownian diffusion coefficient (m^2/s)
$f(\eta)$	= Dimensionless stream function
Nt	= Thermophoresis parameter
P	= Pressure (Pa)
K^*	= Mean absorption coefficient
M	= Magnetic parameter
Cr	= Scaled chemical reaction parameter
B_0	= Magnetic field strength
Nr	= Buoyancy ratio parameter
(u,v)	= Velocity components in x- and y-axis (m/s)
C_f	= Skin-friction coefficient
c_p	= Specific heat (J/kg K)

Greek symbols

α	= Thermal diffusivity of base fluid (m^2/s)
ρ_f	= Fluid density (kg m^{-3})
ψ	= Stream function
τ	= Parameter defined by $\varepsilon\,(\rho c)_p/(\rho c)_f$
$\phi\,(\eta)$	= Dimensionless nanoparticle volume fraction Similarity variable
$\theta\,(\eta)$	= Dimensionless temperature
β	= Thermal expansion coefficient (1/K)

Subscripts

w	= Condition at cone surface
η	= Similarity variable
Ra_x	= Convention parameter
Nu_x	= Nusselt number
C_w	= Nanoparticle volume fraction on the cone
(x, y)	= Cartesian coordinates
T_∞	= Ambient temperature attained
K_r	= Chemical reaction parameter
Jw	= Wall mass flux
D_T	= Thermophoretic diffusion coefficient (m^2/s)

a	=	Constant
Le	=	Lewis number
Nb	=	Brownian motion parameter
q_r	=	Radiative heat flux
σ^*	=	Stephan–Boltzman constant
$\mathrm{Sh_x}$	=	Sherwood number
Pr	=	Prandtl number
R	=	Radiation parameter
τ_{w}	=	Skin-friction coefficient
ν	=	Kinematic viscosity of the base fluid ($m^2 s^{-1}$)
$(\rho c_p)_{\mathrm{f}}$	=	Heat capacitance of the base fluid (J/m^3 K)
$(\rho c_p)_{\mathrm{p}}$	=	Heat capacitance of the nanofluid
η	=	Similarity variable
$(\rho)_{\mathrm{p}}$	=	Density of the nanofluid
σ	=	Electrical conductivity
∞	=	Condition far away from cone surface
f	=	Base fluid

1. Introduction

The theory of nanofluids is an old concept, and it was first introduced by Choi and Eastman (1995) when they were researching on new coolants and cooling technologies, and it became popular because of its numerous applications in heat exchangers, nuclear reactor systems, boilers, electronic cooling and energy storage devices (Ostrach, 1988). The thermal conductivity and ultra-small particle size are the valuable thermophysical properties of nanofluids, and because of this, nanofluids show significantly better performance than the normal single- and multi-phase fluids (Li *et al.*, 2009; Buongiorno and Venerus, 2009; Lazarus Godson *et al.*, 2010; Ghadimi *et al.*, 2011). Many theoretical and experimental studies have suggested that thermal conductivity and dynamic viscosity depend on the shape, size and constructive materials of nanoparticles and the type and working temperature of the base fluid (Saidur *et al.*, 2011; Kleinstreuer and Feng, 2011; Abu-Nada, 2009; Sundar *et al.*, 2013; Li and Peterson, 2007). There are some other important mechanisms, methods of synthesis of nanofluid and sonication time, that influence the thermophysical properties and the heat transfer enhancement of nanofluids. In addition, Brownian motion and thermophoresis are the mass transfer mechanisms that affect the convective heat transfer performance of nanofluids (Kuznetsov *et al.*, 2010; Zaraki *et al.*, 2015). Many experimental and numerical studies in the literature have mentioned about the importance of nanofluids' natural convection heat transfer property (Muthtamilselvan *et al.*, 2010; Parvin *et al.*, 2012; Kamyar *et al.*, 2012). However, we can witness diverse conclusions in those experimental and numerical investigations (Haddad *et al.*, 2012). In an experimental investigation of nanofluids, deterioration in the natural convection heat transfer is usually noticed, whereas in numerical investigation, enhancement is reported. In his benchmark study, Buongiorno (2006) reported seven possible mechanisms associating the natural convection of nanofluids with the movement of nanoparticles in the base fluid by using scale analysis. These mechanisms include nanoparticle size, inertia, particle agglomeration, Magnus effect, volume fraction of the nanoparticle, Brownian motion, particle size, and thermophoresis. Among these mechanisms, the Brownian motion and thermophoresis are found to be of importance. The thermophoresis acts against a temperature gradient, aiding the movement of the particles from higher- to lower-temperature regions. In addition, the Brownian motion aids the movement of particles from higher- to lower-concentration areas. Kuznetsov *et al.*

(2010) discussed the influence of the Brownian motion and thermophoresis on nanofluids' natural convection boundary layer flow over a vertical plate, and because of the importance of the Brownian motion and thermophoresis effects, they studied the concentration boundary layer of nanoparticles. Aziz and Khan (2012) presented nanofluids' natural convection boundary layer flow over a vertical plate subject to the convective boundary conditions.

In recent years, it has been found that magneto-nanofluids are significant in many areas of science and technology, with applications in optical modulators, magneto-optical wavelength filters, tunable optical fiber filters and optical switches. Magnetic nanoparticles are especially useful in biomedicine, sink float separation, cancer therapy, etc. Specific biomedical applications involving nanofluids include hyperthermia, magnetic cell separation, drug delivery and contrast enhancement in magnetic resonance imaging. In view of the aforementioned applications, Chamkha *et al.* (2011) studied the mixed-convection magnetohydrodynamic flow of a nanofluid past a stretching permeable surface in the presence of the Brownian motion and thermophoresis effects. Rashidi *et al.* (2014a, 2014b) discussed the dynamics of nanofluids from a non-linearly stretching sheet with transpiration using Homotopy simulation. Rashidi *et al.* (2014a, 2014b) studied single- and double-phase models of nanofluid heat transfer in Wavy Channel. Noghrehabadi and Behseresht (2013) analyzed how flow and heat transfer are affected by variable properties of nanofluids over a vertical cone saturated in a porous medium. Noghrehabadi *et al.* (2013a, 2013b, 2013c) analyzed the natural convection of nanofluids under different geometries of the stretching sheet and a vertical plate. Behseresht *et al.* (2013) presented natural convection heat and mass transfer of nanofluid over a vertical cone by considering the practical range of nanofluids' thermo-physical properties. Chamkha *et al.* (2013) discussed the mixed-convection flow over a vertical cone through a porous medium saturated by a nanofluid with thermal radiation. In addition, Gorla *et al.* (2014) studied nanofluids' natural convection boundary layer flow through a porous medium over a vertical cone. Chamkha *et al.* (2014) presented non-Darcy free convective nanofluids along a vertical plate with suction/injection and internal heat generation. Recently, Chamkha *et al.* (2015) investigated non-Newtonian nanofluid natural convection flow over a cone through a porous medium with uniform heat and volume fraction fluxes. Very recently, Garoosi *et al.* (2015a, 2015b) presented natural convection of nanofluids in a square cavity and heat exchangers.

To the best of the authors' knowledge, no studies have assessed the impact of the two slip effects, namely, Brownian motion and thermophoresis, on the natural convection of electrically conducted heat and mass transfer to the nanofluid over a vertical cone in the presence of radiation and chemical reaction; therefore, this problem has been addressed in this study. The transformed boundary layer equations, which represent the flow, temperature and concentration, are solved numerically using finite-element method (FEM). The problem reported in the present study is of immediate interest in the upcoming generation of heat exchange technology, boilers, solar film collectors and geothermal energy storage systems.

2. Mathematical analysis

Figure 1 shows a two-dimensional, study of an electrically conducting heat and mass transfer boundary layer flow of a nanofluid over a vertical cone. The coordinate system is chosen, as the x-axis is coincident with the flow direction over the cone surface. It is assumed that T_w and C_w are the temperature and nanoparticle volume fraction at the surface of the cone ($y = 0$) and T_∞ and C_∞ are the temperature and nanoparticle volume fraction of the ambient fluid, respectively. In the present analysis, the nanoparticles are persuaded in the base fluid according to the Brownian motion and thermophoresis.

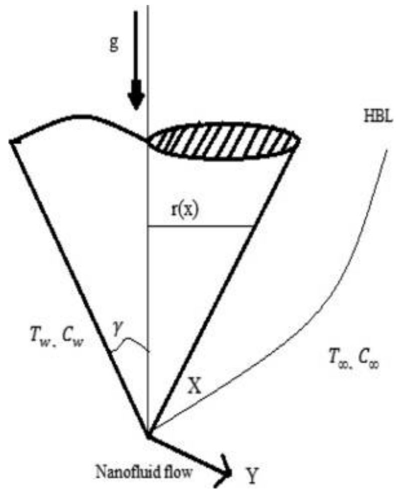

Figure 1.
Physical model and coordinate system

The nanoparticles tend to propel from a hot to cold surface because of thermophoresis. In contrast, the Brownian motion drive nanoparticles to move from higher- to lower-concentration surface. Accordingly, because of the hot surface, nanoparticles move away from the surface of the cone. Because of the Brownian motion force, the concentration of nanoparticles becomes uniform, and the concentration boundary layer of nanoparticles exists over the surface of the cone. Similarly, because of the thermophoresis force, the temperature of nanoparticles becomes uniform; so, a thermal boundary layer of nanoparticles exists at the cone surface. An external magnetic field of strength B_0 is applied in the direction of the *y*-axis. By considering the works of Kuznetsov *et al.* (2010) and by using the Oberbeck–Boussinesq approximation, the governing equations describing the steady-state conservation of mass, momentum and energy, as well as conservation of nanoparticles for nanofluids in the presence of thermal radiation and other important parameters, take the following form:

$$\frac{\partial(ru)}{\partial x} + \frac{\partial(rv)}{\partial y} = 0 \tag{1}$$

$$u\frac{\partial u}{\partial x} + v\frac{\partial u}{\partial y} = \nu\frac{\partial^2 u}{\partial y^2} + g[(1 - C_\infty)\rho_{f\infty}\beta(T - T_\infty) - (\rho_p - \rho_{f\infty})(C - C_\infty)]Cos\gamma - \frac{\sigma B_0^2}{\rho_f}u \tag{2}$$

$$u\frac{\partial T}{\partial x} + v\frac{\partial T}{\partial y} = \alpha\frac{\partial^2 T}{\partial y^2} + \tau\left[D_B\frac{\partial C}{\partial y}.\frac{\partial T}{\partial y} + \left(\frac{D_T}{T_\infty}\right)\left(\frac{\partial T}{\partial y}\right)^2\right] - \frac{1}{\rho c_p}\frac{\partial q_r}{\partial y} \tag{3}$$

$$u\frac{\partial C}{\partial x} + v\frac{\partial C}{\partial y} = D_B\frac{\partial^2 C}{\partial y^2} + \left(\frac{D_T}{T_\infty}\right)\frac{\partial^2 T}{\partial y^2} - K_r(C - C_\infty) \tag{4}$$

The associated boundary conditions are as follows:

$$u = 0, \quad v = 0, \quad T = T_w, \quad C = C_w \qquad at \quad y = 0 \tag{5}$$

$$u \to 0, \quad T \to T_\infty, \quad C \to C_\infty \qquad at \quad y \to \infty \tag{6}$$

The radiative heat flux q_r (using Rosseland Approximation) is defined as follows:

$$q_r = -\frac{4\sigma^*}{3K^*}\frac{\partial T^4}{\partial y}, \tag{7}$$

We assume that the temperature variances inside the flow are such that the term T^4 can be represented as a linear function of temperature, and so, it has the Taylor series expansion. After neglecting higher-order terms from the Taylor series expansion of T^4 about T_∞, we get the following equation:

$$T^4 \cong 4T_\infty^3 T - 3T_\infty^4. \tag{8}$$

Thus, substituting equation (8) in equation (7), we get the following equation:

$$q_r = -\frac{16T_\infty^3\sigma^*}{3K^*}\frac{\partial T}{\partial y}. \tag{9}$$

We now introduce the following similarity variables to transform the governing equations into a system of ordinary differential equations:

$$\begin{gathered} u = axf'(\eta), \quad v = -\sqrt{a\nu}xf(\eta), \quad \eta = \sqrt{\frac{a}{\nu}}y, \\ \theta(\eta) = \frac{T - T_\infty}{T_w - T_\infty}, \; \phi(\eta) = \frac{C - C_\infty}{C_w - C_\infty}. \end{gathered} \tag{10}$$

Here, r can be approximated by the local radius of the cone, if the thermal boundary layer is thin, and is related to the x coordinate by $r = xsin\gamma$.

Substituting equations (9) and (10) into equations (1)-(4), we get the following system of non-linear ordinary differential equations:

$$f''' - (f')^2 + ff'' + Ra_x(\theta - Nr\phi) - Mf' = 0 \tag{11}$$

$$(1 + R)\theta'' + Prf\theta' + Nb\theta'\varphi' + Nt(\theta')^2 = 0 \tag{12}$$

$$\varphi'' + Lef\varphi' - Le\,.\,Cr\,.\,\phi + \frac{Nt}{Nb}\theta'' = 0 \tag{13}$$

The transformed boundary conditions are as follows:

$$\begin{gathered} \eta = 0, \quad f = 0, \quad f'(0) = 1, \quad \theta = 1, \quad \phi = 1. \\ \eta \to \infty, \quad f' = 0, \quad \theta = 0, \quad \phi = 0. \end{gathered} \tag{14}$$

where the prime (′) denotes differentiation with respect to η; the significant thermophysical parameters dictating the flow dynamics are defined as follows:

$$Nr = \frac{(\rho_p - \rho_{f\infty})(C_w - C_\infty)}{\rho_{f\infty}\beta(T_w - T_\infty)(1 - C_\infty)}, \quad Nb = \frac{\tau D_B(C_w - C_\infty)}{\alpha}, \quad Nt = \frac{\tau D_T(T_w - T_\infty)}{\alpha T_\infty}$$
$$Le = \frac{\nu}{D_B}, \quad Ra_x = \frac{(1 - C_\infty)g\beta\rho_{f\infty}(T_w - T_\infty)\cos(\gamma)}{a^2 x}, \quad Cr = \frac{K_r}{a}, \quad Pr = \frac{\nu}{\alpha} \tag{15}$$
$$R = \frac{16T_\infty^3\sigma^*}{3K^*k}, \quad M = \frac{\sigma\beta_o^2 x}{\rho Pe_x^{1/2}}.$$

Quantities of practical interest in this problem are the skin-friction coefficient, local Nusselt number Nu_x and the local Sherwood number Sh_x, which are defined as follows:

$$C_f = \frac{2\tau_w}{\rho}, \quad Nu_x = \frac{xq_w}{k(T_w - T_\infty)}, \quad Sh_x = \frac{xJ_w}{D_B(C_w - C_\infty)} \tag{16}$$

The set of ordinary differential equations (11)–(13) is highly non-linear, and therefore, it cannot be solved analytically. The FEM (Bhargava *et al.*, 2009; Bég *et al.*, 2008; Reddy, 1985; Rana and Bhargava, 2012; Rana *et al.*, 2012; Goyal and Bhargava, 2013) has been implemented to solve these non-linear equations.

3. Numerical method of solution

3.1 The finite-element method

The FEM is such a powerful method for solving ordinary and partial differential equations. The basic idea of this method is dividing the whole domain into smaller elements of finite dimensions called finite elements. This method is a good numerical method in modern engineering analysis, and it can be applied for solving integral equations including heat transfer, fluid mechanics, chemical processing, electrical systems and many others. The steps involved in the FEM are as follows.

(1) *Finite-element discretization*: In finite element discretization, the entire interval is divided into a finite number of subintervals and this subinterval is called an element. The set of all these elements is called the finite-element mesh.

(2) *Generation of the element equations*:
- A variational formulation of the mathematical model over the typical element (an element from the mesh) is performed.
- An approximate solution of the variational problem is assumed, and the element equations are made by substituting this solution in the above system.
- Using interpolating polynomials, the stiffness matrix is constructed.

(3) *Assembly of element equations*: By imposing the inter-element continuity conditions, all the algebraic equations are assembled. This result in a large number of algebraic equations called global FEM, and it represents the whole domain.

(4) *Imposition of boundary conditions*: The boundary conditions which represent the flow model are imposed on the assembled equations.

(5) *Solution of assembled equations*: The assembled equations so obtained can be solved by any of the numerical techniques, namely, Gauss elimination method, LU decomposition method, etc. An important consideration is that of the shape functions which are used to approximate actual functions.

For the solution of system of non-linear ordinary differential equations (11)-(13) together with boundary conditions (14), we first assume that:

$$\frac{\mathrm{df}}{\mathrm{d}\eta} = \mathrm{h} \tag{17}$$

Equations (11)-(13) are then reduced to the following equations:

$$h'' - h^2 + fh' + Ra_x(\theta - Nr\phi) - Mh = 0 \tag{18}$$

$$(1 + R)\theta'' + Prf\theta' + Nb\,\theta'\varphi' + Nt(\theta')^2 = 0 \tag{19}$$

$$\varphi'' + Lef\varphi' - Le\,.\,Cr\,.\,\phi + \frac{Nt}{Nb}\theta'' = 0 \tag{20}$$

The boundary conditions take the following form:

$$\begin{gathered} f = 0, \quad h = 1, \quad \theta = 1, \quad \varphi = 1, \quad at \quad \eta = 0, \\ h = 0, \quad \theta = 0, \quad \varphi = 0, \quad at \quad \eta \to \infty. \end{gathered} \tag{21}$$

3.2 Variational formulation

The variational form associated with equations (17)-(20) over a typical linear element (η_e, η_{e+1}) is given by the following equations:

$$\int_{\eta_e}^{\eta_{e+1}} w_1\left(\frac{\mathrm{df}}{\mathrm{d}\eta} - \mathrm{h}\right)\mathrm{d}\eta = 0 \tag{22}$$

$$\int_{\eta_e}^{\eta_{e+1}} w_2(h'' - h^2 + fh' + Ra_x(\theta - Nr\phi) - Mh)\mathrm{d}\eta = 0 \tag{23}$$

$$\int_{\eta_e}^{\eta_{e+1}} w_3((1 + R)\theta'' + Prf\theta' + Nb\,\theta'\varphi' + Nt(\theta')^2)\mathrm{d}\eta = 0 \tag{24}$$

$$\int_{\eta_e}^{\eta_{e+1}} w_4\left(\varphi'' + Le\,f\,\varphi' - Le.Cr.\phi + \frac{Nt}{Nb}\,\theta''\right)\mathrm{d}\eta = 0 \tag{25}$$

Where w_1, w_2, w_3 and w_4 are arbitrary test functions and may be viewed as the variations in f, h, θ and φ, respectively.

3.3 Finite-element formulation

The FEM may be obtained from the aforementioned equations by substituting finite-element approximations of the following form:

$$f = \sum_{j=0}^{2} f_j\Psi_j, \quad h = \sum_{j=0}^{2} h_j\Psi_j, \quad \theta = \sum_{j=0}^{2} \theta_j\Psi_j, \quad \phi = \sum_{j=0}^{2} \phi_j\Psi_j \tag{26}$$

With $w_1 = w_2 = w_3 = w_4 = \Psi_i, \qquad (i = 1, 2).$

Where Ψ_i is the shape function for a typical element (η_e, η_{e+1}) and is defined as follows:

$$\Psi_1^e = \frac{(\eta_{e+1} - \eta)}{(\eta_{e+1} - \eta_e)}, \quad \Psi_2^e = \frac{(\eta - \eta_e)}{(\eta_{e+1} - \eta_e)}, \quad \eta_e \leq \eta \leq \eta_{e+1}. \tag{27}$$

The FEM of the equations thus formed is given by the following equation:

$$\begin{bmatrix} [K^{11}] & [K^{12}] & [K^{13}] & [K^{14}] \\ [K^{21}] & [K^{22}] & [K^{23}] & [K^{24}] \\ [K^{31}] & [K^{32}] & [K^{33}] & [K^{34}] \\ [K^{41}] & [K^{42}] & [K^{43}] & [K^{44}] \end{bmatrix} \begin{bmatrix} f \\ h \\ \theta \\ \phi \end{bmatrix} = \begin{bmatrix} \{r^1\} \\ \{r^2\} \\ \{r^3\} \\ \{r^4\} \end{bmatrix}$$

Where $[K^{mn}]$ and $[r^m]$ (m, $n = 1, 2, 3, 4$) are defined as follows:

$$K_{ij}{}^{11} = \int_{\eta_e}^{\eta_{e+1}} \Psi_i \frac{\partial \Psi_j}{\partial \eta} \mathrm{d}\eta, K_{ij}{}^{12} = -\int_{\eta_e}^{\eta_{e+1}} \Psi_i \Psi_j \,\mathrm{d}\eta, \; K_{ij}{}^{13} = K_{ij}^{14} = 0.$$

$$K_{ij}{}^{21} = \int_{\eta_e}^{\eta_{e+1}} \psi_i \psi_j \,\mathrm{d}\eta, \quad K_{ij}^{22} = -\int_{\eta_e}^{\eta_{e+1}} \frac{\partial \psi_i}{\partial \eta} \frac{\partial \psi_j}{\partial \eta} \mathrm{d}\eta + \int_{\eta_e}^{\eta_{e+1}} \psi_i \, \psi_j{}^2 \mathrm{d}\eta$$

$$+ M \int_{\eta_e}^{\eta_{e+1}} \psi_i \, \psi_j \mathrm{d}\eta,$$

$$K_{ij}{}^{23} = -Ra_x \int_{\eta_e}^{\eta_{e+1}} \psi_i \psi_j \,\mathrm{d}\eta, \; K_{ij}^{24} = Ra_x * Nr \int_{\eta_e}^{\eta_{e+1}} \psi_i \psi_j \,\mathrm{d}\eta.$$

$$K_{ij}{}^{31} = Pr \int_{\eta_e}^{\eta_{e+1}} \psi_i \, \theta^{-} \; \psi_j \mathrm{d}\eta, \; K_{ij}^{32} = 0$$

$$K_{ij}^{33} = (1 + R) \int_{\eta_e}^{\eta_{e+1}} \frac{\partial \psi_i}{\partial \eta} \frac{\partial \psi_j}{\partial \eta} \quad \mathrm{d}\eta + Nt \int_{\eta_e}^{\eta_{e+1}} \psi_i \bar{\theta} \frac{\partial \psi_j}{\partial \eta} \quad \mathrm{d}\eta,$$

$$K_{ij}{}^{34} = Nb \int_{\eta_e}^{\eta_{e+1}} \psi_i \, \bar{\phi} \frac{\partial \psi_j}{\partial \eta} \,\mathrm{d}\eta, \quad K_{ij}{}^{41} = \frac{1}{2} Le \int_{\eta_e}^{\eta_{e+1}} \psi_i \, \bar{\phi} \, \psi_j \,\mathrm{d}\eta, \; K_{ij}^{42} = 0,$$

$$K_{ij}^{43} = -\frac{Nt}{Nb} \int_{\eta_e}^{\eta_{e+1}} \frac{\partial \psi_i}{\partial \eta} \frac{\partial \psi_j}{\partial \eta} \mathrm{d}\eta, \; K_{ij}^{44} = \int_{\eta_e}^{\eta_{e+1}} \frac{\partial \psi_i}{\partial \eta} \frac{\partial \psi_j}{\partial \eta} \mathrm{d}\eta - \mathrm{Le}\,.\,\mathrm{Cr} \int_{\eta_e}^{\eta_{e+1}} \psi_i \, \psi_j \mathrm{d}\eta$$

$$r_i^2 = 0, \; r_i^2 = -\left(\Psi_i \frac{d\Psi_i}{d\Psi} \right)_{\eta_e}^{\eta_{e+1}}, \; r_i^3 = -\left(\Psi_i \frac{d\Psi_i}{d\Psi} \right)_{\eta_e}^{\eta_{e+1}}, \; r_i^4 = -\left(\Psi_i \frac{d\Psi_i}{d\Psi} \right)_{\eta_e}^{\eta_{e+1}}$$

Where:

$$\bar{f} = \sum_{j=0}^{2} f_i \frac{\partial \Psi_i}{\partial \eta}, \; \bar{h} = \sum_{j=0}^{2} h_i \frac{\partial \Psi_i}{\partial \eta}, \; \bar{\theta} = \sum_{j=0}^{2} \theta_i \frac{\partial \Psi_i}{\partial \eta}, \; \bar{\phi} = \sum_{j=0}^{2} \phi_i \frac{\partial \Psi_i}{\partial \eta}.$$

The important aspect in this numerical procedure is to select an approximate finite value of η_∞. So, to estimate the relevant value of η_∞, the solution process has been started with an initial value of $\eta_\infty = 4$, and then equations (22)-(25) are solved with associated boundary conditions. We have updated the value of η_∞ and the solution process is continued until the results are not affected with further values of η_∞. The choice of $\eta_{max} = 5\,and = 8$ for velocity and temperature and concentration has confirmed that all the numerical solutions approach the asymptotic values at the free stream conditions. To investigate the sensitivity of the solutions to mesh density, we have performed the grid invariance test for velocity, temperature and concentration distributions, and the results of the test are shown in Table I. It is observed from this table that in the same domain, the accuracy is not affected, even though the number of elements increases, by decreasing the size of the elements.

4. Results and discussion

Comprehensive numerical computations are conducted for different values of the parameters that describe the flow characteristics, and the results are illustrated graphically from Figures 2-19. In most practical situations, heat should be detached from the hot surface into the ambient space; so, it is worth mentioning that a cone with a hot surface is more practical than that with a cold surface. However, there are some cases in which there is heat reaction or heat absorbing process inside the cone in which the cone should be heated from the ambient space. Hence, the main aim of the present study is to discuss the heat and mass transfer characteristics over a cone with hot surface. The results of this study are compared with those of previously published work and are shown in Table II.

The influence of magnetic field parameter (M) on velocity, temperature and concentration profiles in the boundary layer is depicted in Figures 2–4. It is noticed from these figures that

	f'				θ				ϕ			
	Step size (h)											
η	0.04	0.02	0.01	0.005	0.04	0.02	0.01	0.0005	0.04	0.02	0.01	0.0005
0.0	1.0000	1.0000	1.0000	1.0000	1.0000	1.0000	1.0000	1.0000	1.0000	1.0000	1.0000	1.0000
1.0	0.2712	0.2635	0.2366	0.2365	0.4575	0.4803	0.5004	0.5003	0.4731	0.4734	0.4738	0.4739
2.0	0.0757	0.0715	0.0712	0.0711	0.1558	0.1562	0.1563	0.1562	0.2130	0.2136	0.2137	0.2138
3.0	0.0244	0.0215	0.0211	0.0211	0.0426	0.0428	0.0429	0.0429	0.0857	0.0861	0.0862	0.0862
4.0	0.0102	0.0101	0.0101	0.0101	0.0102	0.0104	0.0104	0.0104	0.0264	0.0265	0.0265	0.0265
5.0	0.0000	0.0000	0.0000	0.0000	0.0013	0.0014	0.0015	0.0015	0.0115	0.0116	0.0116	0.0116
6.0	–	–	–	–	0.0009	0.0010	0.0010	0.0010	0.0011	0.0012	0.0012	0.0012
7.0	–	–	–	–	0.0002	0.0003	0.0003	0.0003	0.0002	0.0003	0.0003	0.0003
8.0	–	–	–	–	0.0000	0.0000	0.0000	0.0000	0.0000	0.0000	0.0000	0.0000

Notes: M = 0.5, Ra_x = 0.5, Nr = 0.5, R = 0.5, Nt = 0.5, Nb = 0.5, Le = 2.0, Cr = 0.2

Table I. Grid-invariance test for velocity distribution (f'), temperature distribution (θ) and concentration distribution (ϕ)

Nr	$-\theta'(0)$ Gorla and Chamkha (2011)	Present study	$-\phi'(0)$ Gorla and Chamkha (2011)	Present study
0.0	0.32790	0.32784	1.49867	1.49781
0.1	0.32633	0.32598	1.48416	1.48394
0.2	0.32462	0.32405	1.46816	1.46789
0.3	0.32244	0.32229	1.45266	1.45214
0.4	0.32093	0.32125	1.43639	1.43598
0.5	0.31859	0.31868	1.41950	1.41938

Table II. Comparison of $-\theta'(0)$ and $-\phi'(0)$ for $\gamma = 0$ (plate) and for different values of Nr

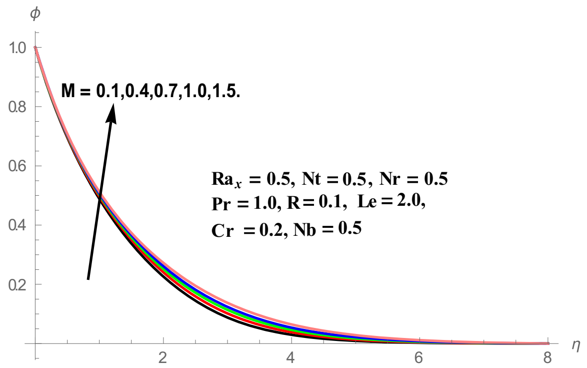

Figure 4.
Effect of M on concentration profile

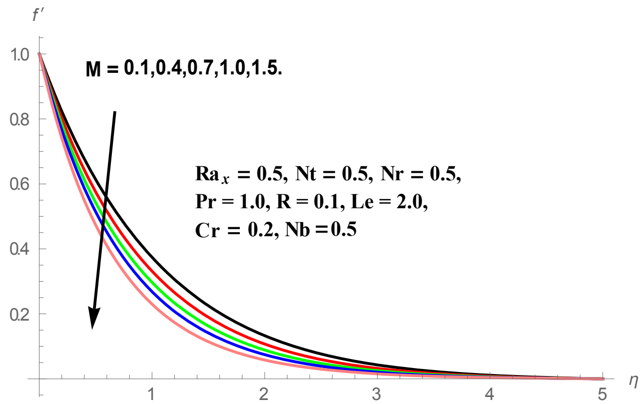

Figure 2.
Effect of M on velocity profile

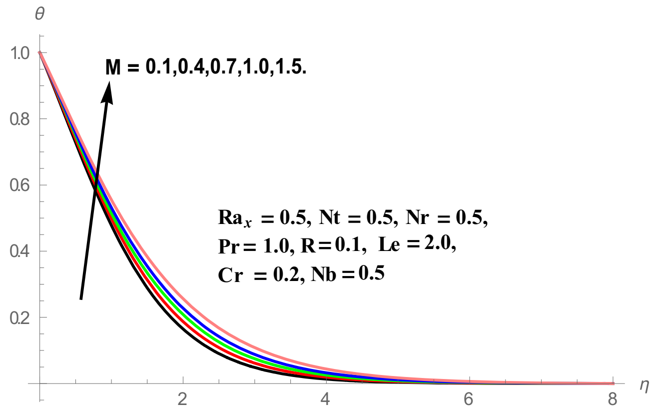

Figure 3.
Effect of M on temperature profile

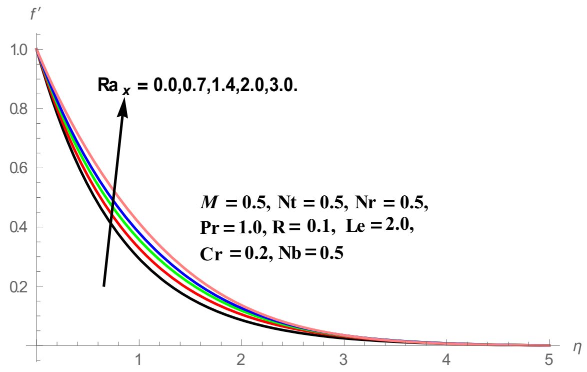

Figure 5.
Effect of Ra_x on velocity profile

the hydrodynamic boundary layer thickness decelerates, whereas thermal boundary layer thickness and solutal boundary layer thickness heighten with enhances in the values of (M). This is because of the fact that the presence of a magnetic field in an electrically conducting fluid produces a force called Lorentz force; this force acts against the flow direction and causes depreciation in velocity profiles (Figure 2), and, at the same time, to overcome the drag force imposed by the Lorentzian retardation, the fluid has to perform extra work. This supplementary work can be converted into thermal energy which increases the temperature of the fluid (Figure 3) and also increases the concentration profiles (Figure 4).

Figures 5-7 depict the effect of convection parameter (Ra_x) on velocity, temperature and concentration distributions. An increase in (Ra_x) elevates the velocity of the fluid because of the enhancement of convection currents (Figure 5). It is analyzed that both temperature and concentration profiles decelerate with increasing values of the convection parameter Ra_x. This is because of the fact that the convection parameter is more dominant as compared to the buoyancy ratio parameter, so that, there is retardation in the thickness of thermal and solutal boundary layers. Furthermore, the temperature and concentration profiles increase when $Ra_x = 0$ (forced convection) because of no buoyancy forces, and both profiles retard with the increasing values of (Ra_x).

Figures 8-10 illustrate the effect of buoyancy ratio parameter (Nr) on velocity, temperature and concentration distributions through the boundary layer regime. It can be seen from Figure 8 that the thickness of hydrodynamic boundary layer is reduced with enhancing values (Nr). The temperature profiles of the fluid increases with increasing values of buoyancy ratio parameter (Nr). This is from the reality that higher values of buoyancy ratio parameter enhance the fluids temperature, so that thermal boundary layer thickness increases (Figure 9). The concentration profiles enhance throughout the fluid region for different improving values of the buoyancy ratio parameter (Nr). This is because of the fact that solutal boundary layer thickness elevates with increasing values of Nr (Figure 10).

The effect of thermal radiation parameter (R) on velocity, temperature and concentration profiles is shown in Figures 11-13. It is noticed from Figures 11 and 12 that the hydrodynamic and thermal boundary layer thickness is enhanced with the higher values of (R) in the entire flow region. This is because of the fact that imposing thermal radiation into the flow, will increase the temperature of the fluid, causing an increment in the velocity of the fluid and a further increase in the temperature of the fluid. However, there is deceleration in the concentration boundary layer thickness with increasing values of R (Figure 13).

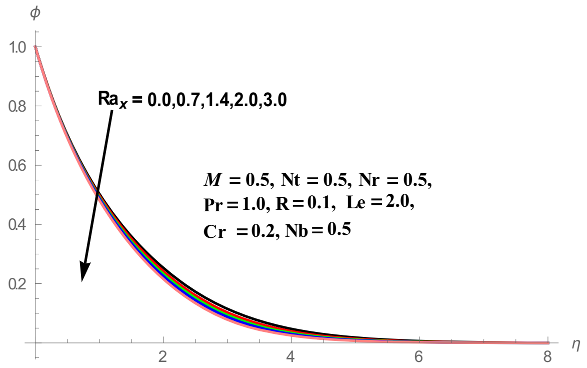

Figure 7. Effect of Ra_x on concentration profile

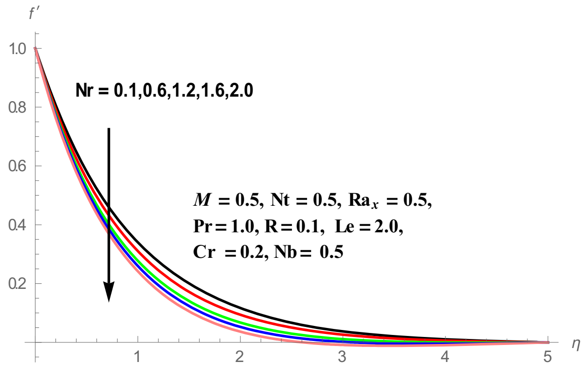

Figure 8. Effect of Nr on velocity profile

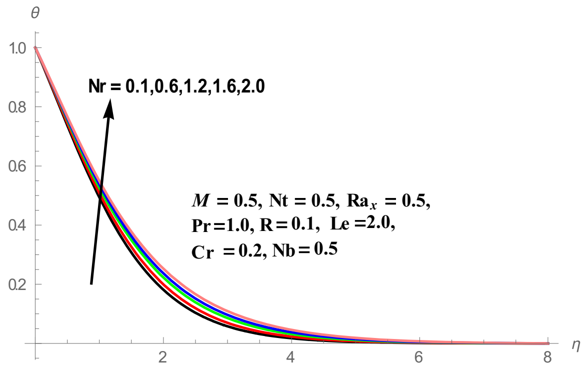

Figure 9. Effect of Nr on temperature profile

Variation of non-dimensional temperature and concentration distributions for different values of thermophoretic parameter (Nt) is depicted in Figures 14 and 15. The thermophoresis acts against the temperature gradient, so that, the particles move from higher- to lower-temperature regions. It is noticed from these figures that both temperature and concentration profiles get elevated in the boundary layer region for the higher values of thermophoretic parameter (Nt). This is from the reality that particles near the hot surface

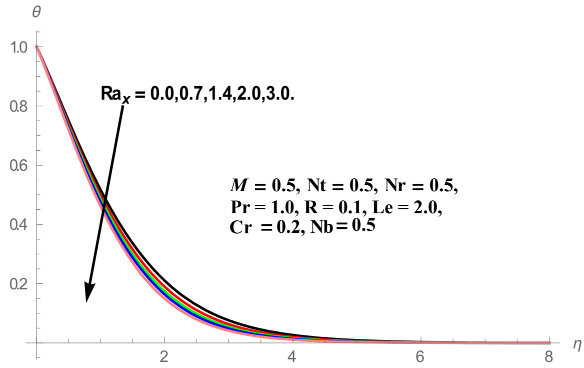

Figure 6.
Effect of Ra_x on temperature profile

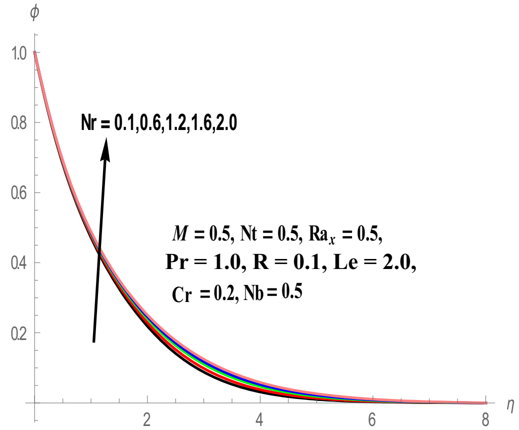

Figure 10.
Effect of Nr on concentration profile

create a thermophoretic force; this force enhances the temperature and concentration of the fluid in the boundary layer region.

The effect of the Brownian motion parameter (Nb) on temperature and concentration profiles is illustrated in Figures 16 and 17. The Brownian motion is the random motion of suspended nanoparticles in the base fluid and is more influenced by its fast-moving atoms or molecules in the base fluid. It is worth mentioning that Brownian motion is related to the size of nanoparticles that are often in the form of agglomerates and/or aggregates. It is noticed that, with the increasing values of Brownian motion parameter (Nb), the temperature profiles also enhance as shown in Figure 16, whereas concentration profiles get depreciated (Figure 17). Clearly, we noticed that the Brownian motion parameter has a significant influence on both temperature and concentration profiles.

The impact of the Lewis number (Le) on concentration profiles is plotted in Figure 18. It is observed that concentration distributions decelerate with the increasing values of the Lewis number in the entire boundary layer region. By definition, the Lewis number represents the ratio of the thermal diffusivity to the mass diffusivity. Increasing the Lewis number means a higher thermal diffusivity and a lower mass diffusivity, and this produces a thinner concentration boundary layer. Figure 19 depicts the variations in concentration distributions in the boundary layer region for different values of the chemical reaction parameter (Cr). We

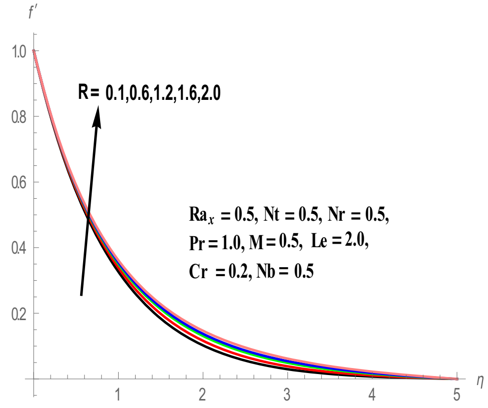

Figure 11.
Effect of R on velocity profile

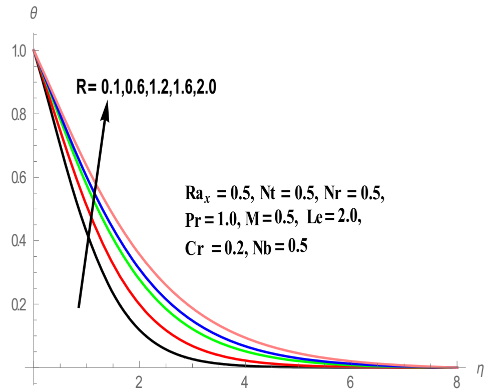

Figure 12.
Effect of R on temperature profile

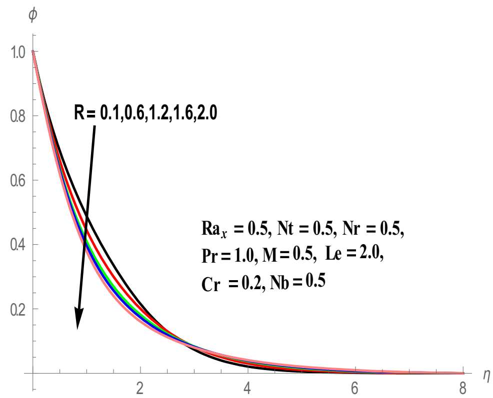

Figure 13.
Effect of R on concentration profile

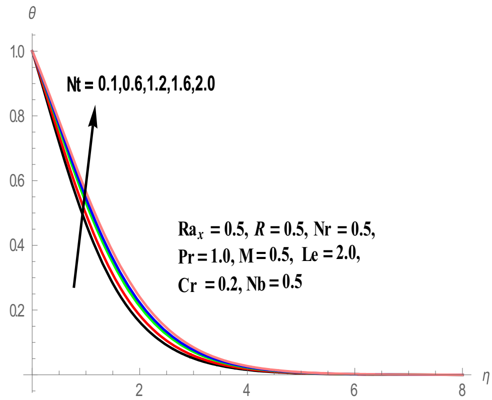

Figure 14.
Effect of *Nt* on temperature profile

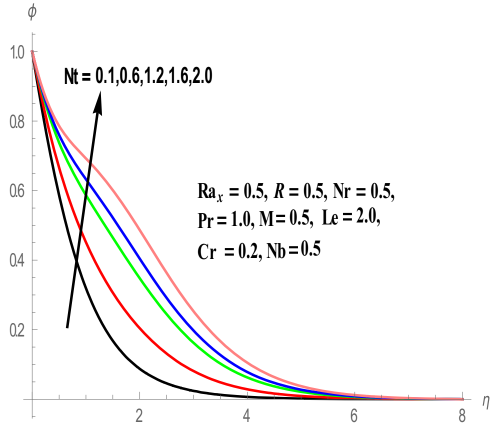

Figure 15.
Effect of *Nt* on concentration profile

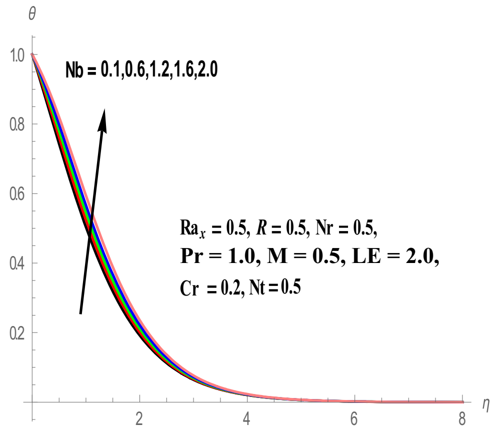

Figure 16.
Effect of *Nb* on temperature profile

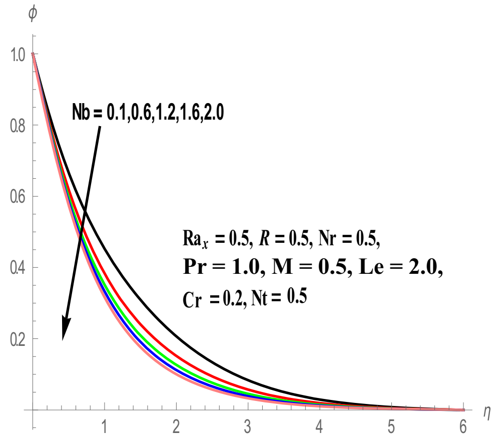

Figure 17.
Effect of *Nb* on concentration profile

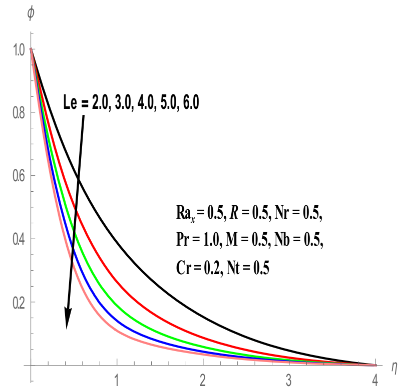

Figure 18.
Effect of *Le* on concentration profile

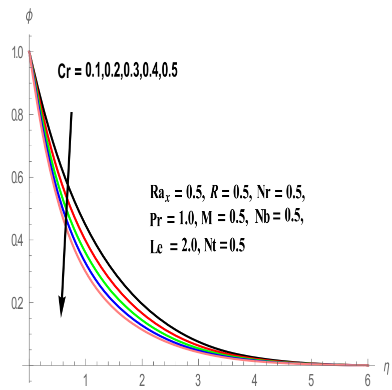

Figure 19.
Effect of *Cr* on concentration profile

see from this figure that the concentration profiles are highly influenced and are decelerated with the higher values of the chemical reaction parameter.

The values of skin-friction coefficient $-f''(0)$, Nusselt number $-\theta'(0)$ and Sherwood number $-\phi'(0)$ are calculated for diverse values of the parameters that entered into the problem when the cone surface is hot and are shown in Table III. It is evident that skin-friction coefficient enhances, whereas the Nusselt number and Sherwood number decelerates with the increasing values of both parameters (M and Nr). It is also seen that the skin-friction coefficient and Nusselt number decreases, whereas Sherwood number elevates with the higher values of (R). We have noticed depreciation in skin-friction coefficient, Nusselt number and Sherwood number with an increment in the values of (Nt) in the entire boundary layer region. With the higher values of the Brownian motion parameter (Nb), the rate of change of velocity and heat transfer rates decelerates, whereas mass transfer rates enhance in the boundary layer regime. It is observed from this table that both skin-friction coefficient and Nusselt number diminish, while the Sherwood number enhances with the improving values of chemical reaction parameter (Cr).

5. Conclusion

In this present study, we have numerically examined the electrically conducting natural convection nanofluid boundary layer flow of heat and mass transfer along a vertical cone with thermal radiation and chemical reaction. The slip of the flow in this problem is because of the Brownian motion and thermophoresis. The powerful mathematical tool similarity variables approach is applied to convert the governing equations into the set of ordinary differential equations. These equations are solved numerically using FEM. The important results of the present study can be summarized as follows.

M	Nr	R	Nt	Nb	Cr	$-f''(0)$	$-\theta'(0)$	$-\phi'(0)$
0.1	0.5	0.1	0.5	0.5	0.2	0.976224	0.517279	0.738589
0.4	0.5	0.1	0.5	0.5	0.2	1.110412	0.497377	0.726902
0.7	0.5	0.1	0.5	0.5	0.2	1.231896	0.479657	0.717882
1.0	0.5	0.1	0.5	0.5	0.2	1.343567	0.463737	0.710818
0.5	0.1	0.1	0.5	0.5	0.2	1.096252	0.498856	0.772449
0.5	0.6	0.1	0.5	0.5	0.2	1.177676	0.484109	0.763795
0.5	1.2	0.1	0.5	0.5	0.2	1.261639	0.466640	0.754750
0.5	1.6	0.1	0.5	0.5	0.2	1.304647	0.456524	0.750177
0.5	0.5	0.1	0.5	0.5	0.2	1.120620	0.553439	0.777955
0.5	0.5	0.6	0.5	0.5	0.2	1.106437	0.481675	0.820010
0.5	0.5	1.2	0.5	0.5	0.2	1.093811	0.419854	0.856753
0.5	0.5	1.6	0.5	0.5	0.2	1.088752	0.395820	0.870976
0.5	0.5	0.1	0.1	0.5	0.2	1.109380	0.545613	0.954760
0.5	0.5	0.1	0.6	0.5	0.2	1.108952	0.494290	0.812529
0.5	0.5	0.1	1.2	0.5	0.2	1.107875	0.438150	0.703462
0.5	0.5	0.1	1.6	0.5	0.2	1.107291	0.417932	0.677069
0.5	0.5	0.1	0.5	0.1	0.2	1.148416	0.487364	0.809419
0.5	0.5	0.1	0.5	0.6	0.2	1.139752	0.431585	0.909090
0.5	0.5	0.1	0.5	1.2	0.2	1.134029	0.380205	0.952647
0.5	0.5	0.1	0.5	1.6	0.2	1.129435	0.333681	0.976201
0.5	0.5	0.1	0.5	0.5	0.1	1.147894	0.487007	0.784499
0.5	0.5	0.1	0.5	0.5	0.2	1.144011	0.482534	0.925675
0.5	0.5	0.1	0.5	0.5	0.3	1.140938	0.478960	1.047727
0.5	0.5	0.1	0.5	0.5	0.4	1.138416	0.476007	1.156171

Table III. The values of skin-friction coefficient $(-f''(0))$, Nusselt number $(-\theta'(0))$ and Sherwood number $[-\phi'(0)]$ for different values of M, Nr, R, Nt, Nb, Cr

- The velocity distributions are reduced, while temperature and concentration profiles elevate with a higher (M).
- With the improving values of (R), the velocity and temperature sketches improve, while concentration distributions are lowered in the boundary layer region.
- The temperature and concentration profiles are elevated in the boundary layer region for higher values of (Nt).
- With the increasing values of (Nb), temperature profiles are enhanced, whereas concentration profiles get depreciated in the flow region.
- Skin-friction coefficient, Nusselt number and Sherwood number diminish with an increase in the values of (Nt) in the entire boundary layer region.
- The skin-friction coefficient and Nusselt number decrease, although Sherwood number increases with the higher values of (R).

References

Abu-Nada, E. (2009), "Effects of variable viscosity and thermal conductivity of Al2O3 – water nanofluid on heat transfer enhancement in natural convection", *International Journal of Heat and Fluid Flow*, Vol. 30 No. 4, pp. 679-690.

Aziz, A. and Khan, W.A. (2012), "Natural convective boundary layer flow of a nanofluid past a convectively heated vertical plate", *International Journal of Thermal Sciences*, Vol. 52, pp. 83-90.

Bég, O.A, Takhar, H.S., Bhargava, R., Rawat, S. and Prasad, V.R. (2008), "Numerical study of heat transfer of a third grade viscoelastic fluid in non-Darcian porous media with thermophysical effects", *Physica Scripta*, Vol. 77, pp. 1-11.

Behseresht, A., Noghrehabadi, A. and Ghalambaz, M. (2013), "Natural-convection heat and mass transfer from a vertical cone in porous media filled with nanofluids using the practical ranges of nanofluids thermo-physical properties", *Chemical Engineering Research and Design*, Vol. 92 No. 3, pp. 447-452.

Bhargava, R., Sharma, R. and Bég, O.A. (2009), "Oscillatory chemically-reacting MHD free convection heat and mass transfer in a porous medium with Soret and Dufour effects: finite element modeling", *International Journal of Applied Mathematics and Mechanics*, Vol. 5 No. 6, pp. 15-37.

Buongiorno, J. (2006), "Convective transport in nanofluids", *Journal Heat Transfer*, Vol. 128, pp. 240-250.

Buongiorno, J. and Venerus, D.C. (2009), "A benchmark study on the thermal conductivity of Nanofluids", *Journal of Applied Physics*, Vol. 106.

Chamkha, A.J., Abbasbandy, S. and Rashad, A.M. (2015), "Non-Darcy natural convection flow of Non-Newtonian nanofluid over a cone saturated in a porous medium with uniform heat and volume fraction fluxes", *International Journal of Numerical Methods for Heat and Fluid Flow*, Vol. 25 No. 2, pp. 422-437.

Chamkha, A.J., Abbasbandy, S., Rashad, A.M. and Vajravelu, K. (2013), "Radiation effects on mixed convection about a cone embedded in a porous medium filled with a nanofluid", *Meccanica*, Vol. 48 No. 2, pp. 275-285.

Chamkha, A.J., Aly, A.M. and Al-Mudhaf, H. (2011), "Laminar MHD mixed convection flow of a nanofluid along a stretching permeable surface in the presence of heat generation or absorption effects", *International Journal of Microscale and Nanoscale Thermal and Fluid Transport Phenomena*, Vol. 2 No. 1, pp. 51-70.

Chamkha, A.J., Rashad, A.M., RamReddy, Ch. and Murthy, P.V. (2014), "Effect of suction/injection on free convection along a vertical plate in a nanofluid saturated non-Darcy porous medium with internal heat generation", *Indian Journal of Pure and Applied Mathematics*, Vol. 45 No. 3, pp. 321-341.

Choi, S.U.S. and Eastman, J.A. (1995), "Enhancing thermal conductivity of fluids with nanoparticles", *International Mechanical Engineering Congress and Exhibition*, San Francisco, CA.

Garoosi, F., Bagheri, G. and Rashidi, M.M. (2015a), "Two phase simulation of natural convection and mixed convection of the nanofluid in a square cavity", *Powder Technology*, Vol. 275, pp. 239-256.

Garoosi, F., Jahanshaloo, L., Rashidi, M.M., Badakhsh, A. and Ali, M.A. (2015b), "Numerical simulation of natural convection of the nanofluid in heat exchangers using a Buongiorno model", *Applied Mathematics and Computation*, Vol. 254, pp. 183-203.

Ghadimi, A., Saidur, R. and Metselaar, H.S.C. (2011), "A review of nanofluid stability properties and characterization in stationary conditions", *International Journal of Heat and Mass Transfer*, Vol. 54, pp. 4051-4068.

Gorla, R.S.R. and Chamkha, A.J. (2011), "Natural convective boundary layer flow over a horizontal plate embedded in a porous medium saturated with a nanofluid", *Journal of Modern Physics*, Vol. 2, pp. 2-71.

Gorla, R.S.R., Chamkha, A.J. and Ghodeswar, V. (2014), "Natural convective boundary layer flow over a vertical cone embedded in a porous medium saturated with a nanofluid", *Journal of Nanofluids*, Vol. 3, pp. 65-71.

Goyal, M. and Bhargava, R. (2013), "Numerical solution of MHD viscoelastic nanofluid flow over a stretching sheet with partial slip and heat source/sink", *ISRN Nanotechnology*, doi: 10.1155/2013/931021.

Haddad, Z., Oztop, H.F., Abu-Nada, E. and Mataoui, A. (2012), "A review on natural convective heat transfer of nanofluids", *Renewable and Sustainable Energy Reviews*, Vol. 16 No. 7, pp. 5363-5378.

Kamyar, A., Saidur, R. and Hasanuzzaman, M. (2012), "Application of computational fluid dynamics (CFD) for nanofluid", *International Journal of Heat and Mass Transfer*, Vol. 55, pp. 4104-4115.

Kleinstreuer, C. and Feng, Y. (2011), "Experimental and theoretical studies of nanofluids thermal conductivity enhancement: a review", *Nanoscale Research Letters*, Vol. 6, p. 229.

Kuznetsov, A.V. and Nield, D.A. (2010), "Natural convective boundary-layer flow of a nanofluid past a vertical plate", *International Journal of Thermal Sciences*, Vol. 49 No. 2, pp. 243-247.

Lazarus, G.A., Balakrishnan, R., Dhasan, M.L. and Wongwises, S. (2010), "Enhancement of heat transfer using nanofluids – an overview", *Renewable and Sustainable Energy Reviews*, Vol. 14 No. 2, pp. 629-641.

Li, C.H. and Peterson, G.P. (2007), "The effect of particle size on the effective thermal conductivity of Al_2O_3-water nanofluids", *Journal of Applied Physics*, Vol. 101, pp. 1-5.

Li, Y., Zhou, J., Tung, S., Schneider, E. and Xi, S. (2009), "A review on development of nanofluid preparation and characterization", *Powder Technol*, Vol. 196 No. 2, pp. 89-101.

Muthtamilselvan, M., Kandaswamy, P. and Lee, J. (2010), "Heat transfer enhancement of copper-water nanofluids in a lid-driven enclosure", *Communications in Nonlinear Science and Numerical Simulation*, Vol. 15 No. 6, pp. 1501-1510.

Noghrehabadi, A. and Behseresht, A. (2013), "Flow and heat transfer affected by variable properties of nanofluids in natural-convection over a vertical cone in porous media", *Computers & Fluids*, Vol. 88, pp. 313-325.

Noghrehabadi, A., Behseresht, A. and Ghalambaz, M. (2013a), "Natural convection of nanofluid over vertical plate embedded in porous medium: prescribed surface heat flux", *Applied Mathematics and Mechanics*, Vol. 34 No. 6, pp. 669-686.

Noghrehabadi, A., Pourrajab, R. and Ghalambaz, M. (2013b), "Effect of partial slip boundary condition on the flow and heat transfer of nanofluids past stretching sheet prescribed constant wall temperature", *International Journal of Thermal Sciences*, Vol. 54, pp. 253-261.

Noghrehabadi, A., Saffarian, M.R., Pourrajab, R. and Ghalambaz, M. (2013c), “Entropy analysis for nanofluid flow over a stretching sheet in the presence of heat generation/absorption and partial slip”, *Journal of Mechanical Science and Technology*, Vol. 27 No. 3, pp. 927-937.

Ostrach, S. (1988), “Natural convection in enclosures”, *Journal of Heat Transfer*, Vol. 110 No. 4b, pp. 1175-1190.

Parvin, S., Nasrin, R., Alim, M.A., Hossain, N.F. and Chamkha, A.J. (2012), “Thermal conductivity variation on natural convection flow of water–alumina nanofluid in an annulus”, *International Journal of Heat and Mass Transfer*, Vol. 55, pp. 5268-5274.

Rana, P. and Bhargava, R. (2012), “Flow and heat transfer of a nanofluid over a nonlinearly stretching sheet: a numerical study”, *Communications in Nonlinear Science and Numerical Simulation*, Vol. 17 No. 1, pp. 212-226.

Rana, P., Bhargava, R. and Bég, O.A. (2012), “Numerical solution for mixed convection boundary layer flow of a nanofluid along an inclined plate embedded in a porous medium”, *Computers and Mathematics with Applications*, Vol. 64 No. 9, pp. 2816-2832.

Rashidi, M.M., Freidoonimehr, N., Hosseini, A., Bég, O.A. and Hung, T.K. (2014a), “Homotopy simulation of nanofluid dynamics from a non-linearly stretching isothermal permeable sheet with transpiration”, *Meccanica*, Vol. 49 No. 2, pp. 469-482.

Rashidi, M.M., Hosseini, A., Pop, I., Kumar, S. and Freidoonimehr, N. (2014b), “Comparative numerical study of single and two-phase models of nanofluid heat transfer in wavy channel”, *Applied Mathematics and Mechanics (English Edition)*, Vol. 35 No. 7, pp. 831-848.

Reddy, J.N. (1985), *An Introduction to the Finite Element Method*, McGraw-Hill Book, New York, NY.

Saidur, R., Leong, K.Y. and Mohammad, H.A. (2011), “A review on applications and challenges of nanofluids”, *Renewable and Sustainable Energy Reviews*, Vol. 15 No. 3, pp. 1646-1668.

Sundar, L.S., Sharma, K.V., Naik, M.T. and Singh, M.K. (2013), “Empirical and theoretical correlations on viscosity of nanofluids: a review”, *Renewable and Sustainable Energy Reviews*, Vol. 25, pp. 670-686.

Zaraki, A., Ghalambaz, M., Chamkha, A.J., Ghalambaz, M. and de Rossi, D. (2015), “Theoretical analysis of natural convection boundary layer heat and mass transfer of nanofluids: effects of size, shape and type of nanoparticles, type of base fluid and working temperature”, *Advanced Powder Technology*, Vol. 26 No. 3, pp. 935-946.

Corresponding author
P. Sudarsan Reddy can be contacted at: suda1983@gmail.com